

Nanoscale

Accepted Manuscript



This is an *Accepted Manuscript*, which has been through the Royal Society of Chemistry peer review process and has been accepted for publication.

Accepted Manuscripts are published online shortly after acceptance, before technical editing, formatting and proof reading. Using this free service, authors can make their results available to the community, in citable form, before we publish the edited article. We will replace this *Accepted Manuscript* with the edited and formatted *Advance Article* as soon as it is available.

You can find more information about *Accepted Manuscripts* in the [Information for Authors](#).

Please note that technical editing may introduce minor changes to the text and/or graphics, which may alter content. The journal's standard [Terms & Conditions](#) and the [Ethical guidelines](#) still apply. In no event shall the Royal Society of Chemistry be held responsible for any errors or omissions in this *Accepted Manuscript* or any consequences arising from the use of any information it contains.

Cite this: DOI: 10.1039/c0xx00000x

www.rsc.org/xxxxxx

ARTICLE TYPE

Dynamic and static measurement of interfacial capillary forces by a hybrid nanomechanical system

Soyoung Kwon,^a Corey Stambaugh,^{a,b} Bongsu Kim,^a Sangmin An,^a and Wonho Jhe*^a

Received (in XXX, XXX) Xth XXXXXXXXX 20XX, Accepted Xth XXXXXXXXX 20XX

DOI: 10.1039/b000000x

The forces resulting from the presence of interfacial liquids have mechanical importance in ambient condition. For holistic understanding of the liquid-mediated interactions, we combine the force-gradient sensitivity of an atomic force microscope (AFM) with the force measuring capability of a micro-electromechanical force sensor. Simultaneous measurement of the viscoelasticity of water nanomeniscus and the absolute capillary force shows excellent agreement in its entire length, which justifies the validity of the widely used AFM results. We apply the hybrid system to measure the stress and strain, whose hysteretic response provides the intrinsic quantities of the liquid nanocluster.

Introduction

The interaction between surfaces has a major effect on how micro- and nano-scale devices perform; for example, the phenomenon of stiction impacts the repetitive use of nano and micro structures.¹⁻³ It also plays a critical role in the behavior between micro- and nano-scale materials, such as dielectric particles, proteins, and various biomolecules.⁴ The forces involved in the interfacial interaction include the van der Waals, electrostatic, hydration and capillary force.² While these interactions have been studied for a variety of systems, there are still questions regarding the behavior as well as the role of liquids at the interface.^{5,6}

The study of interfacial liquids, in particular at the nanoscale, has usually been done in liquid environments, which allows one to measure various liquid-mediated *continuous* forces and interactions. For example, the surface force apparatus measures the interfacial normal forces, such as the hydration, van der Waals and electrostatic force,⁷ capillary force⁸, in addition to the shear viscoelasticity.⁹ The surface force balance technique also obtains similar normal forces as well as shear forces,^{10,11} suitable for specific understanding of nanotribology.¹² Moreover, various AFM studies in liquid provide viscous and elastic properties of the nanoconfined liquid.^{13,14} The capillary force which plays an important role in interfacial interactions results from either liquid condensation in air or bridging vapor bubble in liquid⁴ and thus deeper understanding of the capillary force remains critical. Therefore, it is important to perform experiments in ambient condition where liquid condensation occurs, where the capillarity is the dominant effect, and also where one can observe phase transition between gas and liquid.

There has been a great interest in the capillary water meniscus formed between two nearby surfaces, which is a ubiquitous form of water in nature in ambient condition¹⁵ and relevant to a variety of nanotechnology applications, for example, its scanning probe

nanolithography applications in oxidation.^{16,17} Special focus has been made on stable formation of the nanometric water meniscus as well as accurate measurement of its viscoelastic and hydrodynamic forces.¹⁸ However, due to the *discontinuous* behavior associated with condensation or rupture of the meniscus, one cannot simply integrate the AFM results to obtain the corresponding capillary force¹⁹; a shortcoming in numerous works on the AFM measurement of the viscosity and elasticity of the meniscus made in ambient condition.^{20,21} Moreover, it is a great experimental challenge to directly measure the normal force of the meniscus. Therefore, for holistic understanding, one requires an independent and direct measurement of the capillary force, which can also serve as a justification of the diverse dynamic AFM methods.

In this Letter, we have developed a hybrid system of noncontact AFM and microelectromechanical system (MEMS) to investigate, simultaneously, the dynamic and static forces resulting from the surface-liquid interactions. This system employs a quartz tuning fork (QTF)-based AFM to measure the dynamic response of a nanoscale liquid meniscus of water,^{15,22} while the MEMS force sensor directly measures such static forces as the capillary, adhesion, and hydrodynamic force.^{23,24} In particular, the MEMS sensor provides the absolute value of the capillary forces, and complements the QTF measurement in the *entire* distance range, which provides reaffirming justification of the widely used dynamic AFM results. Moreover, it allows access to multiple driving frequencies, and can measure the stress and strain of the water meniscus. To achieve accurate measurements, careful calibration and analysis of the hybrid system's behavior is first undertaken. We then demonstrate that the MEMS force sensor complements the previously known capabilities of the dynamic QTF-based AFM, and also allows additional information on the intrinsic physical quantities of the meniscus.

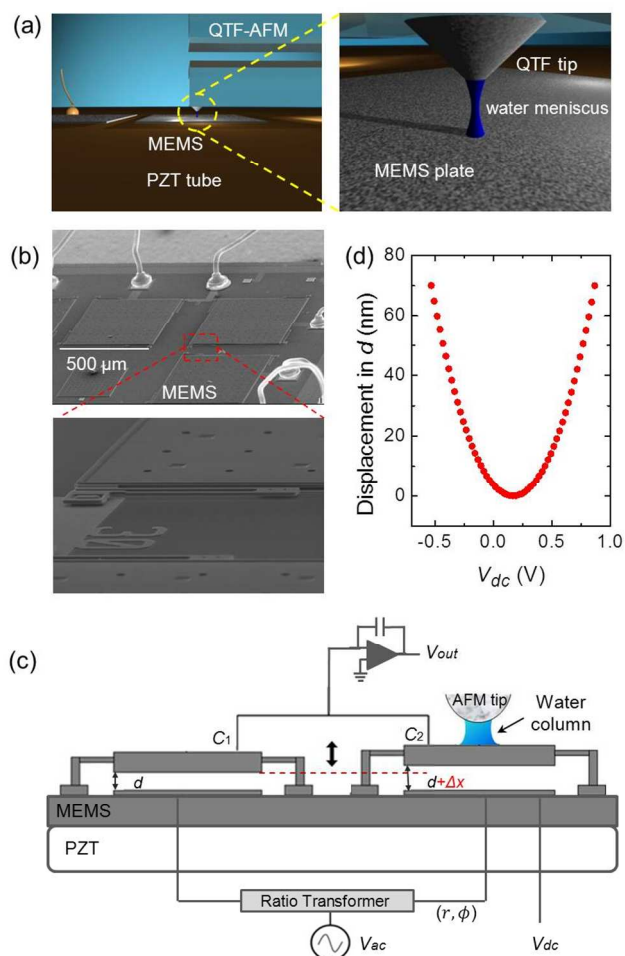


Fig. 1 (a) Cartoon rendition of the hybrid AFM-MEMS system. The enlarged image shows the water nanomeniscus formed between a QTF tip and the MEMS top plate in ambient condition. (b) SEM images of the fabricated MEMS force sensor. (c) Detection scheme of the hybrid system. The output voltage, V_{out} , is initially tuned to zero by balancing the input AC signal, V_{ac} , using a ratio transformer. For small displacements, Δx is linearly proportional to V_{out} . (d) The quadratic calibration curve of the electrostatic force on C_2 . The nanometric displacement in d is plotted versus the DC voltage V_{dc} , where the minimum point (~ 0.2 V) is the residual voltage. The curve also provides the MEMS stiffness, $k_{MEMS} = 2.02 \pm 0.01$ N/m.

15 Experimental

QTF-based AFM

We have used the tapping-mode,^{25,26} noncontact, amplitude-modulation (AM) QTF-based AFM to measure the viscoelasticity of water nanomeniscus.^{15, 27} The QTF provides many useful features for high-resolution experiments, such as a reasonably high quality factor (~ 5000), simple electrical detection and high stiffness ($10^3 \sim 10^4$ N/m) that allows stable formation of the water meniscus at a well-defined height.^{22, 28} In particular, it enables one to avoid the pull-in instability of the probe due to the van der

25 Waals interaction, which generally occurs in the conventional cantilever-based AFM.²² We fabricate the quartz tip by a commercial laser puller (P-2000, Sutter Instruments Co.) to produce the rigid tip with a radius of curvature below 100 nm. Note that while the QTF sensor detects the force gradient in AM-
30 AFM operation and thus provides information on the viscosity as well as the elasticity of the water meniscus,²⁹ it is limited in providing the absolute force with respect to the tip position, which the MEMS force sensor can measure independently.

MEMS

35 The force sensor used in our experiment is a MEMS sensor and actuator, fabricated using the polyMUMPS surface micro-machining process (MEMSCAP Co.). The use of the MEMS sensor provides several unique features such as the ability to easily fabricate duplicates of each structure, and moreover only
40 minimal design modification is needed to produce devices of varying sensitivity.³⁰ Such devices have previously been used for similar studies of mechanical properties. For example, the best known force sensing MEMS is the interfacial force microscope that utilizes a torsional type device with an attached tip to
45 investigate interactions with the surface. This type of device is typically operated in a closed-loop feedback where the gap is held fixed by varying the direct current (DC) voltage. Cheneler *et al.* also proposed a device design to use MEMS to monitor the viscoelastic properties of thin films at low frequency.³⁰ Apart
50 from overall methodology, our MEMS device, which consists of hydrophilic surfaces providing more favorable conditions for the nanoscale liquid meniscus than hydrophobic surfaces in air^{31,32}, is focused on measuring the interaction forces associated with the nanomeniscus. The study of the effect of surface conditions on
55 the capillary force as well as condensation with respect to various contact angles is an intriguing topic to be investigated as a continuing future work.

Figure 1(a) shows the schematic of the AFM-MEMS hybrid system that consists of QTF-based AFM and MEMS. The MEMS device, whose scanning electron microscope (SEM) image is presented in Fig. 1(b), is composed of an electrically isolated poly-silicon ground layer and a movable upper layer of poly-silicon ($500 \mu\text{m} \times 500 \mu\text{m}$) suspended by four springs. Figure 1(c) shows the experimental schematic including two identical MEMS devices, one for fixed reference C_1 and the other for force measurement C_2 , which are both mounted on the piezoelectric transducer (PZT) for vertical movement. The output V_{out} is tuned such that its unloaded output is minimized, and in this way the net plate displacement Δx of C_2 provides direct information of the
65 interaction forces for the tip-induced water meniscus. The stiffness of the MEMS, and thus its resonant frequency as well as force sensitivity, can be determined by the calibration curve shown in Fig. 1(d), $k_{MEMS} = 2.02 \pm 0.01$ N/m, which is about 10 times stiffer than the meniscus. During experiments, a static DC
70 voltage is applied to offset any residual voltage (~ 0.2 V).

The detection scheme is based on a differential capacitance measurement technique that optimizes measurement of the plate's net displacement Δx .³³ An alternating current (AC) voltage V_{ac} is applied to each bottom plate of the two capacitors. The phase

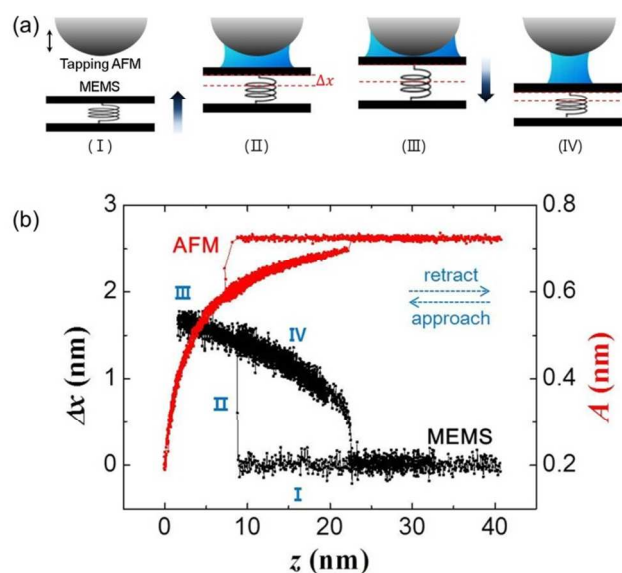


Fig. 2 (a) Experimental procedures: (I) approach of the MEMS sensor by PZT, (II) formation of the water meniscus and instant displacement of the top plate by Δx , (III) incremental change of Δx as the upper plate is further attracted, and (IV) retraction of the MEMS sensor and rupture of the water meniscus. (b) The typical responses of the QTF-based AFM (change of the tip oscillation amplitude A ; red curves) and the MEMS (displacement Δx ; black curves) during approach and subsequent retraction from (I) to (IV). Here, z represents the displacement of the PZT that controls the movement of the MEMS sensor.

difference between the two AC signals is set at 180° and the relative amplitude is finely adjusted using a commercial precision ratio transformer (M-1011A, Tegam Inc.) so as to null the output signal V_{out} , which depends on the difference of the capacitances by, $V_{\text{out}} = V_{\text{ac}}(C_1 - C_2)/\beta$ (β is the charge to voltage factor of the charge sensitive amplifier). Therefore, the output signal of the MEMS sensor picks up any change in C_2 , which is the measure of the meniscus-induced Δx ,

$$\Delta x = \frac{V_{\text{out}} d^2}{\beta^{-1} S \epsilon_0 V_{\text{ac}} - V_{\text{out}} d}, \quad (1)$$

where S is the plate area of each MEMS sensor. When the nanometric water meniscus spontaneously forms between the QTF tip and the top plate of C_2 , it exerts an attractive force on the plate (Fig. 1(c)). This causes the plate to rise up and induces the net displacement Δx , which can be then converted to the actual force exerted by the water column on the movable plate of C_2 ,

$$F_{\text{MEMS}} = -k_{\text{MEMS}} \Delta x. \quad (2)$$

Here the nanometric value of Δx is small enough to place it in the linear regime.

Results and discussion

Figure 2(a) shows the experimental procedures of approach and

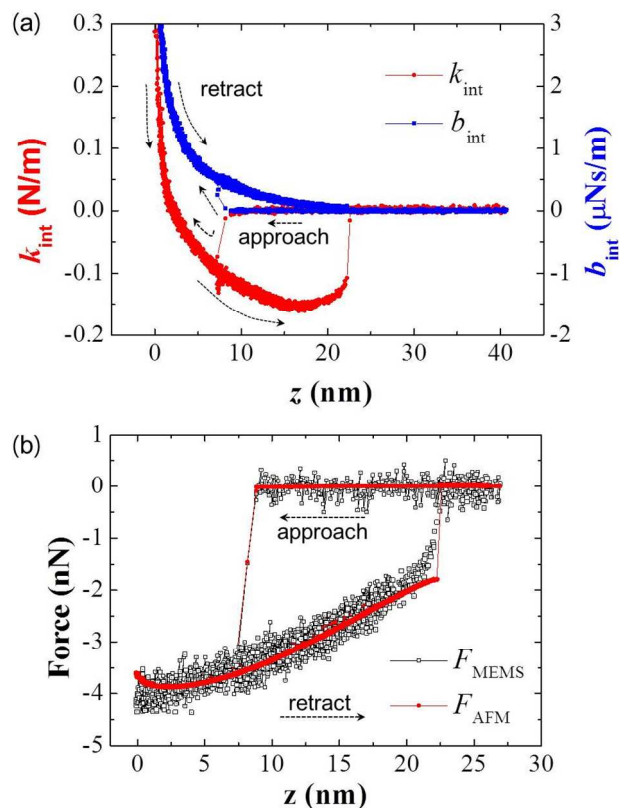


Fig. 3 (a) The effective elasticity k_{int} and damping coefficient b_{int} of the water meniscus obtained by the QTF-based AFM. (b) The calculated interaction forces for the QTF-based AFM (Eq. (3)) as well as the directly measured forces for the MEMS force sensor in the entire approach and retraction procedures, which are in excellent agreement. Here, the adjustable constant F_0 for F_{AFM} is set to -1.8 nN (red curve), which shows the best fit with the MEMS data.

retraction, which is used in our scheme to determine the mechanical properties of nanoscale materials. First, the MEMS plate approaches the QTF probe by incremental movement of the PZT attached below the MEMS device (step I). When the QTF probe and the top plate of the MEMS sensor are within a few nm's, the capillary-condensed nanometric water meniscus suddenly changes the monitoring signals of the QTF and MEMS (step II).¹⁵ The meniscus formation causes the top plate to jump up, resulting in Δx . Continued approach by extension of the PZT brings the tip and upper plate closer (step III). Finally, the mechanical properties of the meniscus are measured while the PZT is subsequently retracted until the water meniscus is stretched and ruptured (step IV). Figure 2(b) presents the typical responses of the system. The oscillation amplitude A of the AFM tip (red curve) and the displacement Δx of the MEMS sensor (black curve) are plotted versus the PZT displacement (z), where the steps (I) to (IV) are indicated.

Figure 3 presents the typical experimental results of the forces obtained by the hybrid AFM-MEMS system. Note that the effect of gravity is completely negligible in this experiment because the capillary force is 9 orders of magnitude greater than the gravity

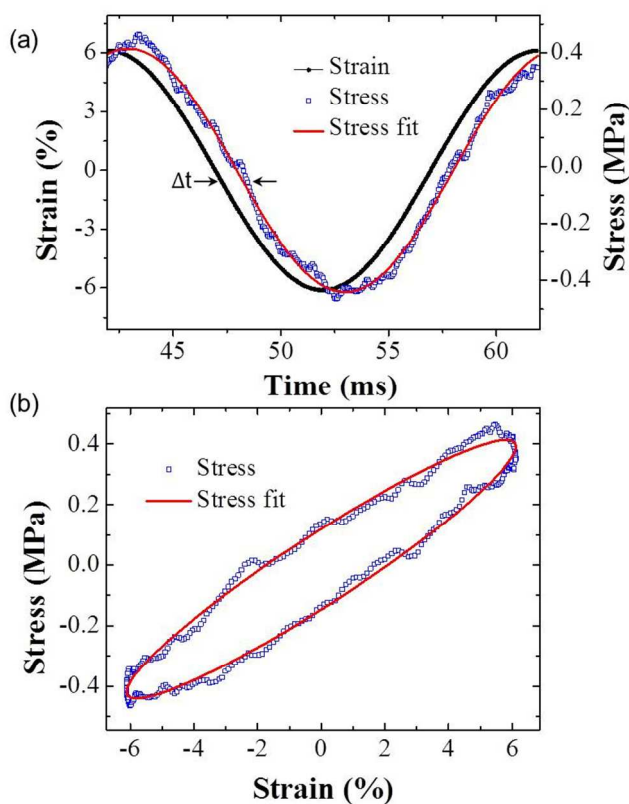


Fig. 4 (a) The temporal responses in the strain and stress measurement of the water nanomeniscus when a sinusoidal potential is applied to the PZT actuator at 50 Hz. The measured time lag (Δt) provides the loss tangent. (b) The stress-strain hysteresis curve. The slope provides the Young's modulus of the water meniscus, whereas the enclosed area measures the energy loss per cycle.

effect estimated for the nanomeniscus volume.³⁴ In Fig. 3(a), the measured amplitude and phase of the QTF-based AFM under small oscillation are converted to the effective elasticity k_{int} and damping coefficient b_{int} of the meniscus.²⁹ They are then integrated to find the corresponding force F_{AFM} , as shown in Fig. 3(b),

$$F_{\text{AFM}} = \int_{Z_r}^Z dz [-k_{\text{int}}] + F_0, \quad (3)$$

where Z_r is the rupture distance and F_0 is a constant of integration. As observed in Fig. 3(a), k_{int} is positive near the substrate while it decreases to negative as the water meniscus is elongated during retraction of the MEMS plates. The positive value of k_{int} in the vicinity of the substrate is attributed to the short-range repulsive hydration force,³⁵ whereas k_{int} is negative in the region relatively far from the surface where the attractive capillary force dominates.¹⁹ The measured damping coefficient is much larger than that expected for bulk water; ~ 80 (30) times larger at the position of meniscus formation (rupture). The resulting viscosity of the water meniscus appears to be much larger than the bulk value even at the distance of 7 nm. This is associated with the surface tension effect of the meniscus, unlike the great enhancement of viscosity that has been usually observed at less than ~ 2 nm distance.^{9, 13} Figure 3(b) provides the MEMS force measurements as well as the calculated force results of the

QTF-based AFM, which are in excellent agreement. This indicates the two approaches are in general not only consistent but complementary with each other.

The capability to measure simultaneously the elasticity, viscosity and force of the water meniscus provides several novel features. Above all, it offers a definite and unambiguous confirmation of what quantities the QTF-based AFM actually measures. In other words, quantitative understanding of the nanometric water meniscus is obtained by simultaneous and direct measurement of the absolute force by the MEMS as well as the dynamic properties (i.e., elasticity and viscosity) by the QTF-based AFM. Furthermore, the hybrid AFM-MEMS provides conclusive evidence for the reliability of previous analyses of QTF-based AFM results, based on the good agreement between the interaction forces obtained by QTF-based AFM and MEMS. In particular, this indicates the water meniscus exhibits static behaviours at the drive frequency (~ 32 kHz) of the QTF.

As an application of the dual capability of the hybrid AFM-MEMS scheme, we have performed a strain and stress measurement of the nanometric water meniscus. The resulting strain-stress curves allow one to obtain the Young's modulus as well as the time-lag response (or loss tangent) of the water meniscus, which provides extended information on the nanometric material. A sinusoidal tensile strain of the stretched or compressed nanomeniscus leads to stress when the stress proceeds ahead of the strain. That is, for the sinusoidal strain $\epsilon(t) = \epsilon_0 \sin(2\pi\nu t)$, the stress becomes $\sigma(t) = \sigma_0 \sin(2\pi\nu t - \delta)$, which is retarded by the phase angle δ . Figure 4(a) shows the measured time delay³⁶ ($\Delta t = \delta/2\pi\nu$) is $(1.01 \pm 0.05) \times 10^{-3}$ s, obtained without using any fitting parameters, which has been so far only calculated indirectly by the AFM method and thus depends on the models used for the specific materials. Figure 4(b) presents the elliptical hysteresis curve between stress and strain,³⁶ which results from the linearly viscoelastic behaviour of the water nanomeniscus. The slope of the hysteresis provides the Young's modulus, or the stress-to-strain ratio, of the meniscus and it is measured as 6.7 ± 0.3 MPa, comparable to that of soft rubber or soft tissues (1–10 MPa).^{2, 37} The enclosed area in the loop, on the other hand, is the strain energy per unit volume released as heat in each cycle, corresponding to internal heat generation. We find the area is $3,041 \pm 150$ J/m³, which is about 40 times larger than the thermal energy for the estimated meniscus volume²² at room temperature (~ 150 J/m³).

In general, the loss tangent (or $\tan\delta$), defined by the ratio of loss modulus to storage modulus, is high ($\gg 1$) for the liquid-like materials whereas it is low ($\ll 1$) for the solid-like ones.³⁸ At the low modulation frequency of 50 Hz in our experiment, we obtain $\tan\delta = 0.33 \pm 0.02$, which indicates the solid-like behaviour of the meniscus. The specific loss tangent value implies that the nanometric water meniscus behaves like a rubbery or viscous material comparable to the hevea rubber³⁶, which represents the interesting and topical aspect of fluidity of the nanoscale water. In particular, for solid-like fluid, the loss modulus is much lower than storage modulus³⁹ and this agrees well with our recent observation that water at the liquid-vapor interface is more rigid or solid-like than that inside the meniscus, as demonstrated by the increasing surface to volume ratio investigated by time-resolved non-contact AFM.³⁹ Notice that

extremely fast modulation can cause solid-like behavior even at the picosecond-scale relaxation time of water.⁴⁰

5 Conclusions

We have presented the unique versatility and complementarity of the hybrid AFM-MEMS scheme, which provides both direct and indirect information of the discontinuous as well as continuous forces associated with the water nanomeniscus. In particular, the MEMS sensor provides the absolute value of the capillary forces, and complements the QTF measurement in the entire distance range, which provides reaffirming justification of the widely used dynamic AFM results. Moreover, it allows access to multiple driving frequencies, and can measure the stress and strain of the water meniscus. Since the MEMS force sensor is also an actuator, an in-depth research on the water meniscus is possible when driven by the actuator itself, which may allow one to measure the effective relaxation time of the nanoconfined liquid in addition to its static properties. Moreover, our demonstrated stress and strain measurement may reveal how nano-liquid behaves differently from bulk as the viscoelasticity is in general enhanced at the nanoscale. One may also explore the diverse liquid-mediated interfacial interactions by fabricating a dual-mode MEMS force sensor, which could be operated for both shear and normal force measurements. The dependence of the frequency on the nanomeniscus behavior is an interesting issue to be addressed for further study. By changing the frequency and the sample materials including biological systems, one can obtain a systematic and quantitative understanding of nanoscale materials which may even contribute to practical applications. Experiment under oscillatory shear motion of the AFM tip is an immediate and interesting candidate to exploit the strength of the hybrid AFM-MEMS system.

Acknowledgments

This work was supported by the National Research Foundation of Korea (NRF) grant funded by the Korea government (MSIP) (No. 2013-056344). C. Stambaugh acknowledges support from NSF-OISE Grant 0853104.

Notes and references

^aDepartment of Physics and Astronomy, Institute of Applied Physics, Seoul National University, Daehak-dong, Gwanak-gu, Seoul 151-747, Korea. Tel: +82 2 880-6600; Fax: +822886-5786; E-mail: whjhe@snu.ac.kr

^bNational Institute of Standards and Technology, MD 20899, USA (Present address).

† Electronic Supplementary Information (ESI) available: [details of any supplementary information available should be included here]. See DOI: 10.1039/b000000x/

- 1 M. Urbakh, J. Klafter, D. Gourdon, and J. Israelachvili, *Nature*, 2004, **430**, 525.
- 2 J. Israelachvili, *Intermolecular and Surface Forces*, Academic Press, New York, 2011.
- 3 K. B. Jinesh and J. W. M. Frenken, *Phys. Rev. Lett.*, 2006, **96**, 166103.

- 4 Y. Min, M. Akbulut, K. Kristiansen, Y. Golan, and J. Israelachvili, *Nature Mater.*, 2008, **7**, 527.
- 5 A. E. Nel, L. Mdlar, D. Velegol, T. Xia, E. M. V. Hoek, P. Somasundaran, F. Klaessig, V. Castranova, and M. Thompson, *Nature Mater.*, 2009, **8**, 543.
- 6 A. Frlich, F. Gabel, M. Jasnin, U. Lehnert, D. Oesterhelt, A. M. Stadler, M. Tehei, M. Weik, K. Wood, and G. Zaccai, *Faraday Discuss.*, 2009, **141**, 117.
- 7 J. N. Israelachvili and G. E. Adams, *Nature*, 1976, **262**, 774.
- 8 H. K. Christenson and P. M. Claesson, *Adv. Colloid Interface. Sci.*, 2001, **91**, 391.
- 9 Y. Zhu and S. Granick, *Phys. Rev. Lett.*, 2001, **87**, 096104.
- 10 N. Kampf, D. Ben-Yaakov, D. Andelman, S. A. Safran, and J. Klein, *Phys. Rev. Lett.*, 2009, **103**, 118304.
- 11 J. Klein and E. Kumacheva, *Science*, 2002, **297**, 1540.
- 12 B. Bhushan, J. Israelachvili, and U. Landman, *Nature*, 1995, **374**, 607.
- 13 S. H. Khan, G. Matei, S. Patil, and P. M. Hoemann, *Phys. Rev. Lett.*, 2010, **105**, 106101.
- 14 T.-D. Li and E. Riedo, *Phys. Rev. Lett.*, 2008, **100**, 106102.
- 15 S. An, C. Stambaugh, G. Kim, M. Lee, Y. Kim, K. Lee, and W. Jhe, *Nanoscale*, 2012, **4**, 6493.
- 16 M. Calleja, M. Tello, and R. García, *J. Appl. Phys.*, 2002, **92**, 5539.
- 17 R. Garcia, M. Calleja and F. Pérez-Murano, *Appl. Phys. Lett.*, 1998, **72**, 2295.
- 18 H. Choe, M.-H. Hong, Y. Seo, K. Lee, G. Kim, Y. Cho, J. Ihm, and W. Jhe, *Phys. Rev. Lett.*, 2005, **95**, 187801.
- 19 C. D. Willett, M. J. Adams, S. A. Johnson, and J. P. K. Seville, *Langmuir*, 2000, **16**, 9396.
- 20 F. Restagno, L. Bocquet, and T. Biben, *Phys. Rev. Lett.*, 2000, **84**, 2433.
- 21 Y. Men, X. Zhang, and W. Wang, *J. Chem. Phys.*, 2009, **131**, 184702.
- 22 M. Lee, B. Sung, N. Hashemi, and W. Jhe, *Faraday Discuss.*, 2009, **141**, 415.
- 23 H. B. Chan and C. Stambaugh, *Phys. Rev. Lett.*, 2007, **99**, 060601.
- 24 M. Bao and H. Yang, *Sens. Actuators A*, 2007, **136**, 3.
- 25 R. Garcia, and R. Perez, *Surf. Sci. Rep.*, 2002, **47**, 197.
- 26 R. Garcia and A. San Paulo, *Phys. Rev. B*, 1999, **60**, 4961.
- 27 M. Lee, J. Jahng, K. Kim, and W. Jhe, *Appl. Phys. Lett.*, 2007, **91**, 023117.
- 28 F. J. Giessibl, *Appl. Phys. Lett.*, 1998, **73**, 3956.
- 29 M. Lee and W. Jhe, *Phys. Rev. Lett.*, 2006, **97**, 036104.
- 30 D. Cheneler, M. Ward, M. Adams, and Z. Zhang, *Sensor Actuat. B-Chem.*, 2008, **130**, 701.
- 31 M. Bingeli and C. M. Mate, *Appl. Phys. Lett.*, 1994, **65**, 415.
- 32 N. V. Zarate, A. J. Harrison, J. D. Litster, and S. P. Beaudoin, *J. Colloid Interface Sci.*, 2013, **411**, 265.
- 33 S. D. Senturia, *Microsystem Design*, Kluwer Academic Publishers, 2001.
- 34 F. M. Orr, L. E. Scriven, and A. P. Rivas, *J. Fluid Mech.*, 1975, **67**, 723.
- 35 J. Faraudo and F. Bresme, *Phys. Rev. Lett.*, 2005, **94**, 077802.
- 36 R. S. Lakes, *Viscoelastic Solids*, CRC Press, 1999.
- 37 C. T. McKee, J. A. Last, P. Russell, and C. J. Murphy, *Tissue Eng. Part B*, 2011, **17**, 155.
- 38 R. G. Larson, *The Structure and Rheology of Complex Fluids*, New York: Oxford University Press, 1999.
- 39 J. Kim, D. Won, B. Sung, and W. Jhe, *J. Phys. Chem. Lett.*, 2014, **5**, 737.
- 40 S. Balasubramanian, C. J. Mundy, and M. L. Klein, *J. Chem. Phys.*, 1996, **105**, 11190.